



# Size Dependent Photocatalytic Activity of ZnO Nanosheets for Degradation of Methyl Red

Abdullah Aljaafari\*

Department of Physics, College of Science, King Faisal University, Al-Ahsa, Saudi Arabia

In this work, ZnO nanosheets with a tunable thickness were produced by a microwave-assisted hydrothermal-based method. The product was well characterized by various tools such as XRD, SEM, EDX spectroscopy, TEM, and Raman spectroscopy. ZnO nanosheets were highly crystalline and possessed a single phase with the wurtzite structure. The ZnO nanosheets have a thickness ranging from 20 to 50 nm, as shown by the micrographs of SEM. The SAED pattern inferred that the ZnO nanosheets have a single crystal nature with preferential growth direction along [0001]. ZnO nanosheets with  $E_2^{\text{high}}$  mode of wurtzite structure were observed by Raman scattering spectra. The photodegradation of methyl red using ZnO nanosheets was measured under UV light irradiation. In comparison with the commercial ZnO, ZnO nanosheets showed higher efficiency in photodegradation of organic dyes. The thinner the nanosheets, the higher their performance, which can be explained based on surface area. The excellent performance of ZnO nanosheets in photodegradable organic dyes might be important in environmental treatment and photocatalysis applications.

## OPEN ACCESS

### Edited by:

Rengaraj Selvaraj,  
Sultan Qaboos University, Oman

### Reviewed by:

Sanjay S. Kolekar,  
Shivaji University, India  
Zinetula Z. Insepov,  
Purdue University, United States

### \*Correspondence:

Abdullah Aljaafari  
aaljaafari@kfu.edu.sa

### Speciality section:

This article was submitted to  
Thin Solid Films,  
a section of the journal  
Frontiers in Materials

Received: 03 June 2020

Accepted: 29 September 2020

Published: 18 November 2020

### Citation:

Aljaafari A (2020) Size Dependent  
Photocatalytic Activity of ZnO  
Nanosheets for Degradation of  
Methyl Red.  
Front. Mater. 7:562693.  
doi: 10.3389/fmats.2020.562693

**Keywords:** ZnO, nanosheets (NSs), photocatalysts, XRD, TEM

## INTRODUCTION

Recently, environmental pollution of organic pollutants by photolysis of wide-gapped semiconductors, have attracted great attention (Linsebigler et al., 1995; Chatterjee and Dasgupta, 2005; Comparelli et al., 2005; Thompson and Yates, 2006). Moreover, these nanostructures provide enhancement in the functional properties for potential applications in the fabrication of nanodevices. In photocatalytic applications, numerous semiconducting nanostructures, including ZnO and TiO<sub>2</sub>, are being used due to their unique properties of low cost, high photosensitivity, non-toxicity and environmentally friendly behavior (Wu and Tseng, 2006; Wang et al., 2007). ZnO has been considered to be a more capable photocatalyst than TiO<sub>2</sub> due to its high surface reactivity resulting from a large number of active surface defect states (Kumar and Rao, 2015). Additionally, the more efficient hydroxyl ion production capability (Carraway et al., 1994) of ZnO provides high reaction and mineralization rates (Poulios et al., 1999; Bohle and Spina, 2009; Wang et al., 2009). The catalytic activity of metal oxide nanostructures is known to depend on surface area and surface defects (Baruah et al., 2008). Among the different dimensions, two-dimensional nanostructures including nanosheets or nanotubes can be considered a new class of nanostructure material due to their high anisotropy, large surface area and nanometer scale thickness, and they have interesting properties (Jang et al., 2006).

The unique structural features of two-dimensional nanomaterials, such as ultrathin thickness and possibly specific open crystal planes, may be useful for a wide range of surface interactions/

interactivity-oriented applications, such as electrodes of dye-sensitive solar cells, gas sensors, supercapacitors, lithium ion batteries, photocatalytic water splitting, photocatalysis, etc. (Hosono et al., 2005; Jing and Zhan, 2008; Liu et al., 2009; Qiu et al., 2010; Zhang et al., 2009a). ZnO crystals are composed of closely packed  $O^{2-}$  layers piled alternatively along the c-axis, producing positively charged Zn-terminated (0001) polar surfaces and negatively charged O-terminated (000 $\bar{1}$ ) polar surfaces (Kong and Wang, 2004). ZnO crystals have a non-central symmetric wurtzite structure. The average surface energy of ZnO for the polar  $\pm\{0001\}$  plane is higher than non-polar  $\{01\bar{1}0\}$ , and  $\{2\bar{1}\bar{1}0\}$  planes. It can be expected that the higher-surface-energy  $\pm(0001)$  surface has much higher amounts of chemical activity (Kong and Wang, 2004).

Therefore, the development of a synthesis technique for the shape and size of tunable ZnO nanostructures is needed. Numerous reports have shown the growth of ZnO nanostructures in various dimensions including nanowires, nanobelts, nanorods, nanosheets, and nanotubes (Huang et al., 2001; Pan et al., 2001; Wu et al., 2002; Tien et al., 2007; Baruah and Dutta, 2009; Becker et al., 2011). Also, ZnO nanosheets have been synthesized by using different chemical and physical methods such as thermal evaporation, chemical vapor deposition (CVD), physical vapor deposition (PVD), electrochemical processes, hydrothermal or solvothermal methods (Zhang et al., 2003; Zeng et al., 2005; Hu et al., 2008; Li et al., 2008; Qiu et al., 2009). However, these methods have disadvantages due to their high-temperatures, vacuum conditions, or longer reaction times, which make these techniques expensive. Thus, to fulfill economic and industrial necessities, a quick and easy process for the synthesis of ZnO nanostructures under ambient conditions is required. Nevertheless, the controlled growths of ZnO nanosheets with the thickness in quantum confinement range and their thickness dependent photocatalytic properties have not been reported. More recently, microwave radiation has introduced the synthesis of nanomaterials. Compared with conventional heating, microwave heating has unique effects such as fast and homogeneous volumetric heating, high reaction rate, short reaction time, improved reaction selectivity, energy saving and low cost (Ahmed et al., 2011).

In this work, a simple microwave-assisted hydrothermal assisted solution method was used to prepare ZnO nanosheets containing highly reactive (0001) facets and tunable thickness. The dependence of photocatalytic degradation of methyl red dye on the thickness of ZnO nanosheets was investigated. It is worth mentioning that the present products possessed higher specific surface areas and smaller nanosheet thicknesses in quantum confinement range than products from both microwave-assisted processes, and hydrothermal (Zhou et al., 2008; Qiu et al., 2010). Most importantly, there is no requirement of further calcination steps to obtain the final product as is required in earlier reports (Dong et al., 2012). The ZnO nanosheets prepared by the present process possessed single-crystallinity, high surface areas, and ultrathin thicknesses, characteristics which are beneficial for photocatalytic applications.

## EXPERIMENTAL DETAILS

The product was synthesized using the microwave hydrothermal method (CEM; MARS 5). Potassium hydroxide (KOH; 99.99%) and Zinc acetate dihydrate ( $Zn(CH_3COO)_2 \cdot 2H_2O$ ; 99.999) were mainly used in experiments. Different molar ratios of 1:2.5 (sample 1), 1:2.75 (sample 2), 1:5 (sample 3) of  $Zn(CH_3COO)_2 \cdot 2H_2O$  and KOH were dissolved in a round-bottom flask which included 100 ml water. The mixture was then transferred to a Teflon-lined digestion vessel of 100 ml and operated at 160°C and 100 psi for 20 min in a microwave system. The operating power used was 1200 W. The temperature was observed during irradiation by a thermocouple fixed into the reference vessel. After the process, the product was allowed to cool down to room temperature. Centrifuge was used to separate the precipitate which was washed with deionized water and absolute ethanol several times. The product was then dried in an oven at 80°C for 24 h.

For photocatalysis experiments, methyl red (MR) was used as a test pollutant. An aqueous solution of MR (10  $\mu M$ ) was used corresponding to ZnO (10 mg). To attain an adsorption-desorption equilibrium, the suspension was then stirred in the dark for 30 min. A mercury lamp of high pressure was used as a light source radiation. After the time interval, 5 ml was withdrawn and centrifuged immediately to remove the photocatalyst particles. Then it was analyzed by a UV-Vis spectrophotometer (Agilent 8453) to observe the spectra MR. For the photocatalytic stability of ZnO nanosheets, a time track of photocatalytic degradation of MR using photocatalyst was conducted.

X-ray diffraction (Phillips X'pert (MPD-3040)) was used to investigate the phase purity of the product obtained with Cu K $\alpha$  radiations ( $\lambda = 1.5406 \text{ \AA}$ ). Field emission electron microscopy (FESEM) images were obtained using a MIRA II LMH microscope and initial synthesis of ZnO was obtained by energy dispersing X-ray spectroscopy (EDX, Inca Oxford) attached to FESEM.

The electron microscopy (TEM) and electron diffraction pattern for the selected area (SAED) and high-resolution transmission electron microscopy (HRTEM) micrographs were obtained using FE-TEM (JEOL/JEM-2100F version). ZnO nanosheets were first dispersed in ethanol solution followed by ultrasound treatment for 10 min for TEM analysis. Furthermore, a fine drop of ZnO suspension was cast onto a carbon-covered copper mesh and then dried in the air before being transferred to the microscope. The Micro-Raman spectrometer (NRS-3100) was used to obtain a phonon vibrational of ZnO nanostructures, with a solid 532 nm primary laser as an excitation source in configuring background dispersion at room temperature. Optical absorption spectra of room temperature were recorded in the range of 200–800 nm using the UV-vis optical spectrophotometer (Agilent-8453). Brunauer-Emmett-Teller (BET) surface area measurements were performed by nitrogen adsorption using Autosorb-1 (Quantachrome Instruments, Boynton Beach, FL, United States).

## RESULTS AND DISCUSSION

XRD patterns of ZnO nanosheets prepared at different KOH concentrations are shown in **Figures 1A**. The diffraction peaks were indexed to the hexagonal wurtzite ZnO phase (JCPDS 89-1397) with calculated lattice parameters  $a$  and  $c$  to be 3.249 and 5.207 Å, respectively. It can also be seen that all the samples showed a single-phase nature with a wurtzite structure (Marković et al., 2019). As the molar ratio was increased from 1:2.5 to 1:5, the peak became more intense which signified better crystallinity.

High-resolution transmission electron microscopy (HRTEM) revealed the atomic structures of ZnO nanosheets. The HRTEM image (**Figures 1B**) also shows that the ZnO nanosheets (sample 1) were highly crystalline, having a lattice spacing of about 0.26 nm, corresponding to the distance between the (002) planes in ZnO crystal lattice. Also, selected-area electron diffraction (SAED) patterns of the same ZnO nanosheets (sample 1) were indexed to hexagonal ZnO, which also indicated that the ZnO nanosheets were single crystalline and had growth along the [001] direction. These results are also in good agreement with the XRD results.

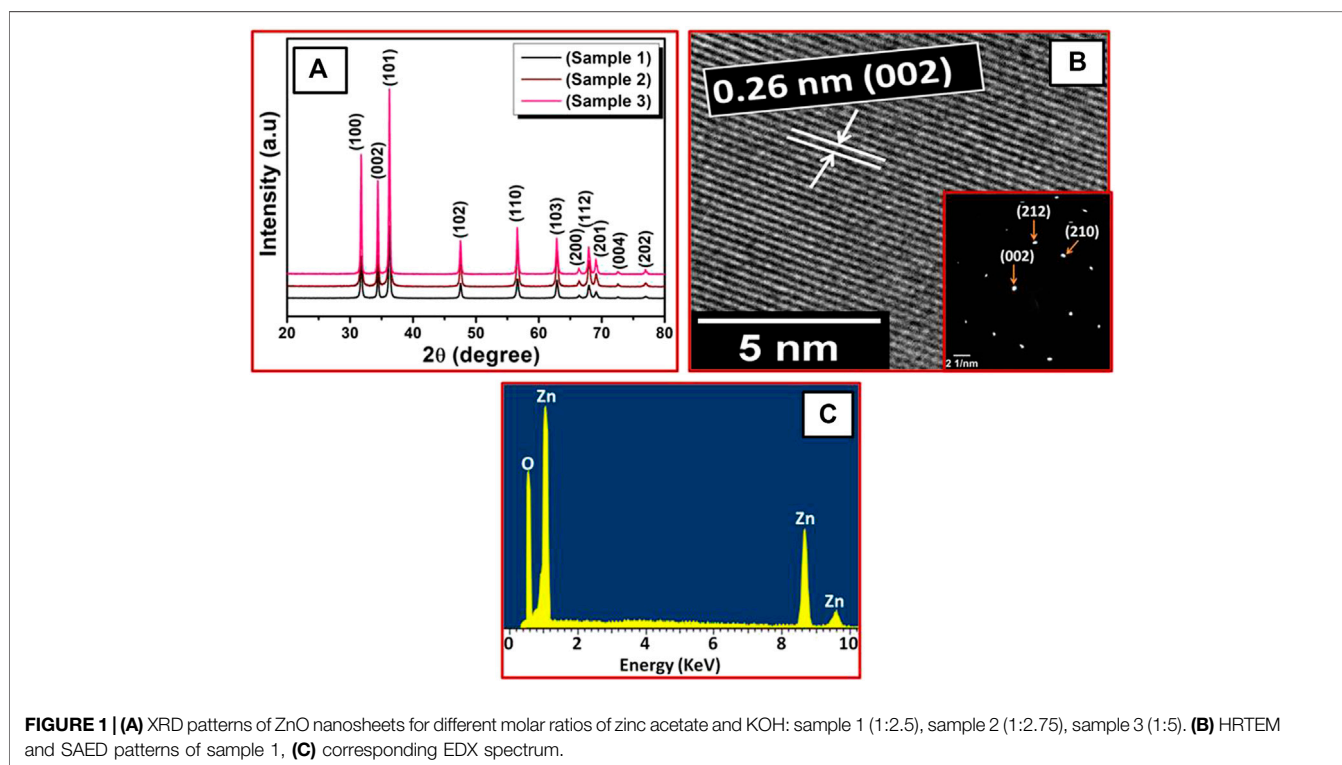
Energy dispersive X-ray spectroscopy (EDX) was used for elemental composition of the ZnO nanosheets. The EDX spectrum (**Figures 1C**) shows peaks of Zn and O for all the ZnO nanosheets, which signifies that the ZnO nanosheets were composed of Zn and O only and no impurity peaks were found, confirming high purity of ZnO nanosheets.

**Figure 2** shows FESEM images of the ZnO nanosheets with different thicknesses obtained from the varying concentration of KOH. **Figures 2A** represents the morphology of the ZnO

nanosheets (sample 1) with a lateral dimension of ~500 nm and thickness of ~24 nm, respectively with a molar ratio of 1:2.5. The thickness of the samples was measured by using “Image J” software which is a strong tool for the TEM and SEM analysis. For the measurement, nanosheets in the images were chosen randomly, and the lateral size and thickness were measured accurately. Using ImageJ, one can measure the size in nano-range with more precision, thus the thickness was reported. With the increase of the molar ratio to 1:2.75 (sample 2), the lateral dimension of nanosheets decreased to ~360 nm, with a slight increase in the thickness to ~29 nm (**Figures 2B**). On further increasing the molar ratio to 1:5 (sample 3) (**Figures 2C**), ZnO nanosheets with lateral dimension ~240 nm, thickness ~50 nm; aspect ratio ~37 were obtained. Hence, it can be seen that as the lateral dimension of the nanosheets decreases, the thickness increases with the increasing molar ratio, concluding that ZnO morphology is molar ratio dependent.

**Figure 3** depicts the room temperature Raman spectra of ZnO nanosheets for different molar ratios of zinc acetate and KOH. The Raman spectrum (**Figure 3**) of ZnO nanosheets confirms conventional vibration modes (Cusco et al., 2007) of  $E_2^{\text{high}}-E_2^{\text{low}}$ ,  $A_1$  (TO), and  $E_2^{\text{high}}$ , centered at  $332\text{ cm}^{-1}$ ,  $381\text{ cm}^{-1}$ , and  $439\text{ cm}^{-1}$ , respectively. These results commensurate with the XRD results. Further, with the increase in molar ratio the intensity of  $E_2^{\text{high}}$  mode varies, this change in the intensity of Raman modes is due to increase in supersaturation (Nagy and Casey, 1971).

To study the specific surface area of the nanosheets with various thicknesses, BET analysis was carried out. BET analysis of the sample one showed a surface area of  $182\text{ m}^2/\text{g}$ ,





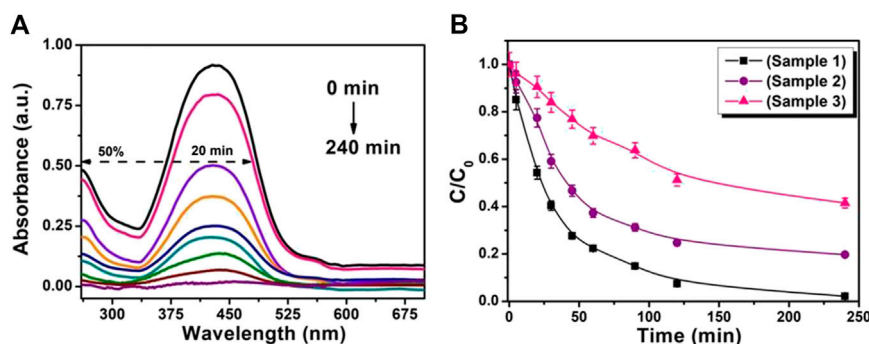


**FIGURE 4 | (A)** UV-visible absorbance spectra of photodegradation of MR in the presence of ZnO nanosheets (sample 1). **(B)** Temporal evolution of MR absorption spectra with various ZnO nanosheets photocatalysts.

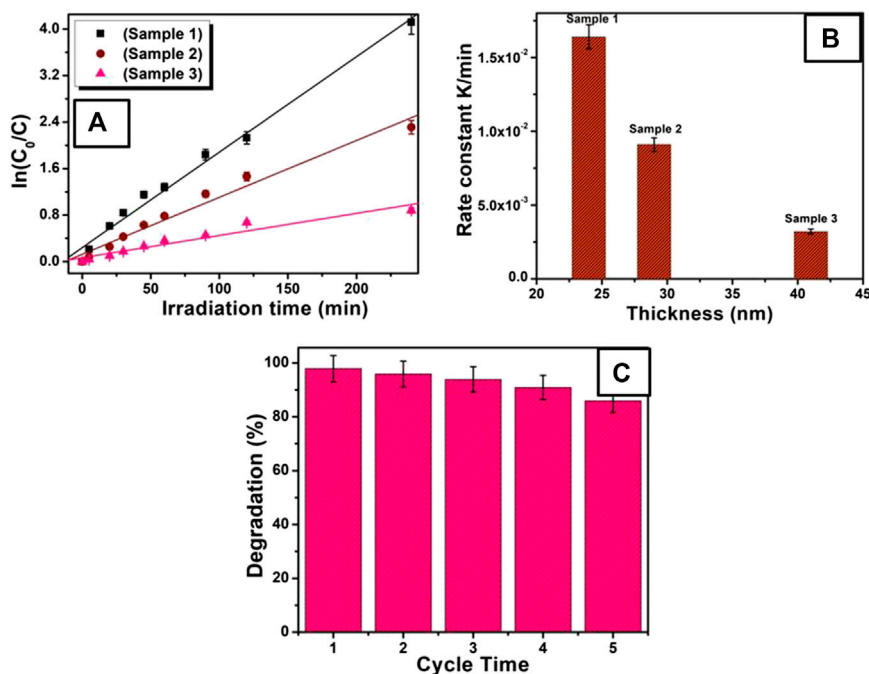


**FIGURE 5 | (A)** Kinetic relationship of  $\ln(C_0/C)$  vs. irradiation time, for various ZnO nanosheet photocatalysts. **(B)** Plot of rate constant vs. thickness of nanosheets. **(C)** The stability of ZnO nanosheets (sample 1) for photodegradation of MR.

photocatalytic process can be regarded as a pseudo-first-order reaction with the rate equation  $\ln(C_0/C) = Kt$ , where,  $t$  is reaction time,  $K$  is the apparent reaction rate constant, and  $C_0$  and  $C$  are the concentration of MR at 0 and  $t$  time, respectively. **Figures 5B** gives the relation between reaction rate  $k$  and nanosheets with different thickness. The apparent reaction rate constant  $K$  for the degradation of MR was calculated to be  $1.60 \times 10^{-2} \text{ min}^{-1}$ ,  $9.10 \times 10^{-3} \text{ min}^{-1}$ , and  $3.18 \times 10^{-3} \text{ min}^{-1}$  for ZnO nanosheets with thicknesses of  $\sim 24$  nm (sample 1),  $\sim 29$  nm (sample 2), and  $\sim 50$  nm (sample 3), respectively. As can be seen from inset of **Figures 5B**, the reaction rate constant is higher for thinner nanosheets (sample 1) than for the thicker one (sample 3), signifying higher photocatalytic activity of thinner ZnO nanosheets.

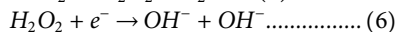
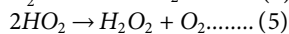
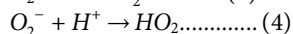
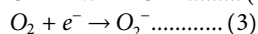
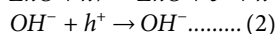
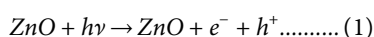
Additionally, comparing the photocatalytic activity of other previously reported nanostructures with the thinner ZnO nanosheets (sample 1) obtained in the present study, it is found that ZnO nanosheets showed better photocatalytic behavior. *Comparelli et al. (2004)* showed the degradation to be 50% of MR with nanosized ZnO, and 90% of MR with nanosized  $\text{TiO}_2$  for 140 min under UV irradiation. *Kanjwal et al. (2010)* showed that the hierarchical nanostructure of ZnO- $\text{TiO}_2$  can remove almost all the MR dye within 90 min of irradiation time; moreover, pure ZnO nanoflowers removed less than 30% of MR dye, even after 180 min. However, for pristine  $\text{TiO}_2$  nanofibers, up to 50% of the dye was removed after 180 min. In the present work, more than 50% of MR was degraded by ZnO nanosheets (sample 1) within 20 min and

almost completely degraded for 240 min of UV light irradiation. Therefore, thin ZnO nanosheets obtained in the present work are far better photocatalysts than others, taking care that the experimental conditions in the above mentioned previous reports might be different.

The main criterion for the development of photocatalysts for organic dye degradation is its stability. In order to estimate the photocatalytic stability of the ZnO nanosheets, a time track for photocatalytic degradation of MR using thin ZnO nanosheets (sample 1) was recorded as shown in **Figures 5C**. For repeated runs, slight change in the degradation of MR was found for the photocatalytic reaction at 60 min, which shows that thinner ZnO nanosheets are stable. So, it can be used as a potential candidate for practical photocatalysis applications.

Several factors such as carrier recombination, size of the particles, surface area, surface acidity, and presence of higher number of hydroxyl groups are responsible for the photocatalytic activity of a catalytic material. In this work, thinner ZnO nanosheets (sample 1) show a higher percentage of degradation as compared to the thicker nanosheets as well as previously reported work. The enhancement of photocatalytic activity can be attributed to the relative increase of the active morphological surface due to the increased surface to volume ratio and low recombination rate of electron hole pairs, generated by optical exposure, owing to largely available surface states.

Photocatalytic degradation process is due to the action of hydroxyl radicals formed during the reaction (Zhang et al., 2009b). The mechanism is as follows: On illumination of ZnO nanosheets with light, electrons get excited from the valence band to the conduction band of ZnO, leaving a hole in the valence band. The hydroxyl groups present on the surface of the ZnO nanosheets react with the photogenerated hole to produce hydroxyl radicals. Also, dissolved oxygen interacts with photogenerated electrons to form peroxide ( $O_2^-$ ). This peroxide takes one proton to form a superoxide ( $HO_2^-$ ) and then hydrogen peroxide ( $H_2O_2$ ).



A hydroxyl radical was also produced by the attack of a photogenerated electron to the hydrogen peroxide. These

reactive radicals and intermediate species react with dye and degrade them into non-toxic organic compounds.

## CONCLUSION

Highly-crystalline ZnO nanosheets with different thicknesses have been prepared by a simple microwave-hydrothermal assisted solution method. XRD, HRTEM, SAED, and Raman analyses explained that ZnO nanosheets are of hexagonal phase structure. FESEM images showed that the thickness of ZnO nanosheets could be efficiently controlled by changing the molar ratio. Increasing the molar ratio increases the thickness of the nanosheets and decreases the lateral dimension. Raman measurements confirmed the characteristic mode  $E_2^{\text{high}}$  of ZnO nanosheets. Photodegradation results show that the thinner ZnO nanosheet (sample 1) is capable of degrading ~50% of MR within 20 min and degrades MR almost completely on increasing irradiation time to 240 min. This improvement in photocatalytic activity might be due to the easy separation of photogenerated charge carriers in the thinner nanosheets which resulted in the enhanced oxygen chemisorptions. Considering this outstanding photocatalytic performance, and simple preparation method, the prepared ZnO nanosheets are believed to have potential applications in photocatalysis and environmental remediation.

## DATA AVAILABILITY STATEMENT

The raw data supporting the conclusions of this article will be made available by the authors, without undue reservation.

## AUTHOR CONTRIBUTIONS

AA designed the experiment to execute the concept. AA performed the analyses, and wrote the manuscript.

## ACKNOWLEDGMENTS

The author would like to thank the Deanship of Scientific Research at King Faisal University for supporting this research through NASHER track (grant # 186106).

## REFERENCES

- Ahmed, F., Kumar, S., Arshi, N., Anwar, M. S., Koo, B. H., and Lee, C. G. (2011). Rapid and cost effective synthesis of zno nanorods using microwave irradiation technique. *Funct. Mater. Lett.* 04, 1–5. doi:10.1142/s1793604711001531
- Baruah, S., and Dutta, J. (2009). Hydrothermal growth of ZnO nanostructures. *Sci. Technol. Adv. Mater.* 10, 013001. doi:10.1088/1468-6996/10/1/013001
- Baruah, S., Rafique, R. F., and Dutta, J. (2008). Visible light photocatalysis by tailoring crystal defects in zinc oxide nanostructures. *Nano* 3, 8.
- Becker, J., Raghupathi, K. R., St. Pierre, J., Zhao, D., and Koodali, R. T. (2011). Tuning of the crystallite and particle sizes of ZnO nanocrystalline materials in solvothermal synthesis and their photocatalytic activity for dye degradation. *J. Phys. Chem. C* 115, 13844. doi:10.1021/jp2038653
- Bohle, D. S., and Spina, C. J. (2009). Cationic and anionic surface binding sites on nanocrystalline zinc oxide: surface influence on photoluminescence and photocatalysis. *J. Am. Chem. Soc.* 131, 4397. doi:10.1021/ja808663b
- Carraway, E. R., Hoffman, A. J., and Hoffmann, M. R. (1994). Photocatalytic oxidation of organic acids on quantum-sized semiconductor colloids, *Environ. Sci. Technol.* 28, 786. doi:10.1021/es00054a007
- Chatterjee, D., and Dasgupta, S. (2005). Visible light induced photocatalytic degradation of organic pollutants, *J. Photochem. Photobiol. C Photochem. Rev.* 6, 186. doi:10.1016/j.jphotochemrev.2005.09.001

- Comparelli, R., Cozzoli, P. D., Curri, M. L., Agostiano, A., Mascolo, G., and Lovecchio, G. (2004). Photocatalytic degradation of methyl-red by immobilised nanoparticles of TiO<sub>2</sub> and ZnO. *Water Sci. Technol.* 49, 183. doi:10.2166/wst.2004.0257
- Comparelli, R., Fanizza, E., Curri, M. L., Cozzi, P. D., Mascolo, G., and Agostiano, A. (2005). Photocatalytic degradation of azo dyes by organic-capped anatase TiO<sub>2</sub> nanocrystals immobilized onto substrates. *Appl. Catal., B* 1, 60.
- Cusco, R., Alarcon-Llado, E., Ibanez, J., Artus, L., Jimenez, J., Wang, B. G., et al. (2007). Temperature dependence of Raman scattering in ZnO. *Phys. Rev. B* 75, 165202. doi:10.1103/physrevb.75.165202
- Dong, J.-Y., Lin, C.-H., Hsu, Y.-J., Lu, S.-Y., and Wong, D. S.-H. (2012). Single-crystalline mesoporous ZnO nanosheets prepared with a green antisolvent method exhibiting excellent photocatalytic efficiencies. *Crystengcomm* 14, 4732–4737. doi:10.1039/c2ce06739k
- Hosono, E., Fujihara, S., Honma, I., and Zhou, H. (2005). The fabrication of an upright-standing zinc oxide nanosheet for use in dye-sensitized solar cells. *Adv. Mater.* 17, 2091–2094. doi:10.1002/adma.200500275
- Hu, J., Zhu, K., Chen, L., Yang, H., Li, Z., Suchopar, A., et al. (2008). Preparation and surface activity of single-crystalline NiO(111) nanosheets with hexagonal holes: a semiconductor nanospanner. *Adv. Mater.* 20, 267–271. doi:10.1002/adma.200701389
- Huang, M. H., Mao, S., Feick, H., Yan, H. Q., Wu, Y. Y., Kind, H., et al. (2001). Room-temperature ultraviolet nanowire nanolasers. *Science* 292, 1897–1899. doi:10.1126/science.1060367
- Jang, E. S., Won, J.-H., Hwang, S.-J., and Choy, J.-H. (2006). Fine tuning of the face orientation of ZnO crystals to optimize their photocatalytic activity. *Adv. Mater.* 18, 3309. doi:10.1002/adma.200601455
- Jing, Z. H., and Zhan, J. H. (2008). Fabrication and gas-sensing properties of porous ZnO nanoplates. *Adv. Mater.* 20, 4547. doi:10.1002/adma.200800243
- Kanjwal, M. A., Barakat, N. A. M., Sheikh, F. A., Park, S. J., and Kim, H. Y. (2010). Photocatalytic activity of ZnO-TiO<sub>2</sub> hierarchical nanostructure prepared by combined electrospinning and hydrothermal techniques. *Macromol. Res.* 18, 233. doi:10.1007/s13233-010-0303-9
- Kong, X. Y., and Wang, Z. L. (2004). Polar-surface dominated ZnO nanobelts and the electrostatic energy induced nanohelices, nanosprings, and nanospirals. *Appl. Phys. Lett.* 84, 975. doi:10.1063/1.1646453
- Kumar, S. G., and Rao, K. S. R. K. (2015). Zinc oxide based photocatalysis: tailoring surface-bulk structure and related interfacial charge carrier dynamics for better environmental applications. *RSC Adv.* 5, 3306. doi:10.1039/c4ra13299h
- Li, G.-R., Lu, X.-H., Zhao, W.-X., Su, C.-Y., and Tong, Y.-X. (2008). Controllable electrochemical synthesis of Ce<sup>4+</sup>-doped ZnO nanostructures from nanotubes to nanorods and nanocages. *Cryst. Growth Des.* 8, 1276. doi:10.1021/cg7009995
- Linsebigler, A., Lu, G., and Yates, J. T. (1995). Photocatalysis on TiO<sub>2</sub> surfaces: principles, mechanisms, and selected results. *Chem. Rev.* 95, 735–758. doi:10.1021/cr00035a013
- Liu, J., Guo, Z., Meng, F., Luo, T., Li, M., and Liu, J. (2009). Novel porous single-crystalline ZnO nanosheets fabricated by annealing ZnS(en)0.5(en = ethylenediamine) precursor. Application in a gas sensor for indoor air contaminant detection. *Nanotechnology* 20, 125501. doi:10.1088/0957-4484/20/12/125501
- Marković, S., Simatović, I. S., Ahmetović, S., Veselinović, L., Stojadinović, S., Rac, V., et al. (2019). Surfactant-assisted microwave processing of ZnO particles: a simple way for designing the surface-to-bulk defect ratio and improving photo(electro)catalytic properties. *RSC Adv.* 9, 17165
- Nagy, G. D., and Casey, E. J. (1971). Wiley, 29–36.
- Pan, Z. W., Dai, Z. R., and Wang, Z. L. (2001). Nanobelts of semiconducting oxides. *Science* 291, 1947. doi:10.1126/science.1058120
- Poulios, I., Makri, D., and Prohaska, X. (1999). Photocatalytic treatment of olive milling waste water: oxidation of protocatechuic acid. *Global Nest: Int. J.* 1, 55.
- Qiu, M., Ye, Z., Lu, J., He, H., Huang, J., Zhu, L., et al. (2009). Growth and properties of ZnO nanorod and nanonails by thermal evaporation. *Appl. Surf. Sci.* 255, 3972. doi:10.1016/j.apsusc.2008.10.093
- Qiu, Y. C., Chen, W., and Yang, S. H. (2010). Facile hydrothermal preparation of hierarchically assembled, porous single-crystalline ZnO nanoplates and their application in dye-sensitized solar cells. *J. Mater. Chem.* 20, 1001. doi:10.1039/b917305f
- Thompson, T. L., and Yates, J. T. (2006). Surface science studies of the photoactivation of TiO<sub>2</sub>New photochemical processes. *Chem. Rev.* 106, 4428. doi:10.1021/cr050172k
- Tien, L. C., Norton, D. P., Pearton, S. J., Wang, H.-T., and Ren, F. (2007). Nucleation control for ZnO nanorods grown by catalyst-driven molecular beam epitaxy. *Appl. Surf. Sci.* 253, 4620. doi:10.1016/j.apsusc.2006.10.012
- Wang, J., Liu, P., Fu, X., Li, Z., Han, W., and Wang, X. (2009). Relationship between oxygen defects and the photocatalytic property of ZnO nanocrystals in nafion membranes. *Langmuir* 25, 1218. doi:10.1021/la803370z
- Wang, Y. W., Zhang, L. Z., Deng, K. J., Chen, X. Y., and Zou, Z. G. (2007). Low temperature synthesis and photocatalytic activity of rutile TiO<sub>2</sub>Nanorod superstructures. *J. Phys. Chem. C* 111, 2709. doi:10.1021/jp066519k
- Wu, J.-J., and Tseng, C.-H. (2006). Photocatalytic properties of nc-Au/ZnO nanorod composites. *Appl. Catal. B Environ.* 66, 51. doi:10.1016/j.apcatb.2006.02.013
- Wu, J.-J., Liu, S.-C., Wu, C.-T., Hen, C. K. H., and Chen, L.-C. (2002). Heterostructures of ZnO-Zn coaxial nanocables and ZnO nanotubes. *Appl. Phys. Lett.* 81, 1312. doi:10.1063/1.1499512
- Zeng, Y.-J., Ye, Z.-Z., Xu, W.-Z., Zhu, L.-P., and Zhao, B.-H. (2005). Well-aligned ZnO nanowires grown on Si substrate via metal-organic chemical vapor deposition. *Appl. Surf. Sci.* 250, 280. doi:10.1016/j.apsusc.2005.03.140
- Zhang, J., Wang, S., Xu, M., Wang, Y., Zhu, B., Zhang, S., et al. (2009a). Hierarchically porous ZnO architectures for gas sensor application. *Cryst. Growth Des.* 9, 3532. doi:10.1021/cg900269a
- Zhang, L.-S., Wong, K.-H., Zhang, D.-Q., Hu, C., Yu, J. C., Chan, C.-Y., et al. (2009b). Zn:In(OH)<sub>y</sub>SzSolid solution nanoplates: synthesis, characterization, and photocatalytic mechanism. *Environ. Sci. Technol.* 43, 7883. doi:10.1021/es902013d
- Zhang, Y., Jia, H. B., Wang, R. M., Chen, C. P., Luo, X. H., Yu, D. P., et al. (2003). Low-temperature growth and Raman scattering study of vertically aligned ZnO nanowires on Si substrate. *Appl. Phys. Lett.* 83, 4631. doi:10.1063/1.1630849
- Zhou, X. F., Hu, Z. L., Fan, Y. Q., Chen, S., Ding, W. P., and Xu, N. P. (2008). Hollow microsphere assembly of ZnO nanosheets. *J. Phys. Chem. C* 112, 11722. doi:10.1016/j.matchemphys.2008.06.025

**Conflict of Interest:** The authors declare that the research was conducted in the absence of any commercial or financial relationships that could be construed as a potential conflict of interest.

Copyright © 2020 Aljaafari. This is an open-access article distributed under the terms of the Creative Commons Attribution License (CC BY). The use, distribution or reproduction in other forums is permitted, provided the original author(s) and the copyright owner(s) are credited and that the original publication in this journal is cited, in accordance with accepted academic practice. No use, distribution or reproduction is permitted which does not comply with these terms.